Thermal analysis and annealing temperature dependence of electrical properties in $Sn_{10}Sb_{20}Se_{70}$ glassy semiconductor

Praveen Kumar · R. Thangaraj · T. Stephen Sathiaraj

Received: 17 May 2008 / Accepted: 12 August 2008 / Published online: 4 September 2008

Abstract The melt-quenched $Sn_{10}Sb_{20}Se_{70}$ sample in the bulk form was used to prepare films on well-cleaned glass substrates by thermal evaporation method. The activation energy for glass transition (apparent) and crystallization has been analyzed by using the Kissinger formulation. The X-ray diffraction study shows the crystallization of Sb_2Se_3 phase in the major proportion as compared to the $SnSe_2$ phase. The SEM images film of the show the appearance of spherical globules upon annealing below the glass transition temperature. The effect of annealing temperature on the electrical and optical properties has been studied. A linear fit between ΔE and E_o is observed, indicating the validity of Meyer–Neldel rule with the change in the annealing temperature.

Introduction

Chalcogenide glasses are very promising materials because of their potential applications in infrared (IR) optics, optical memories, inorganic photoresists, and anti-reflection coatings, etc. [1]. For infrared applications, the material should have large optical transmission window, low material dispersion, low light scattering, and long wavelength multiphonon edge well above the desired IR wavelength along with good thermal, mechanical, and chemical properties. Recent interest in these materials is to investigate new IR material for CO_2 laser power transmitting optical fibers [2]. The transmission window of Ge–Sb–Se glasses limits their utility for CO_2 laser application [3], which had the multiphonon absorption edge at about 16 μm. The occurrence of micro-crystallization during the fiber drawing results in the inhomogeneous optical fibers with loss in the signal due to scattering. To decrease the transmission losses to meet the commercial requirements, new materials were investigated to shift the multiphonon edge to longer wavelengths by several micrometers and also to enhance the thermal and mechanical properties.

The glass formation with the addition of heavier mass elements in chalcogen reduces the optical gap, consequently shifting the transmission window to longer wavelengths. The addition of Sn increases the glass transition temperature, crystallization temperature, anti-crystallization stability, and chemical durability, and shifts the multiphonon absorption edge to longer wavelengths [2]. Our recent work [4, 5] shows that the Sn addition inhibits crystallization, while more addition leads to further crystallization. The results indicate better thermal stability with large glass transition temperatures for the $Sn_{10}Sb_{20}Se_{70}$ chalcogenide glass [5]. Therefore, the present study reports the thermal studies, structure and the effect of thermal annealing on the surface morphology of glassy films. Also, the effect of thermal annealing at different temperatures on the optical and electrical properties has been reported.

Experimental details

Bulk glass of $Sn_{10}Sb_{20}Se_{70}$ was prepared by conventional melt quenching technique as described earlier [4].

P. Kumar · R. Thangaraj (✉)
Semiconductors Laboratory, Department of Applied Physics, Guru Nanak Dev University, Amritsar 143005, India
e-mail: rthangaraj@rediffmail.com

T. Stephen Sathiaraj
Department of Physics, University of Botswana, Gaborone, Botswana

Differential scanning calorimetric (DSC) studies were carried out using Perkin Elmer (DSC/TGA/DTG, Pyris Diamond) instrument at different heating rates. Approximately 15 mg of the powdered sample with 10 mg of alumina powder as reference were taken in Al pans for each DSC runs. The temperature and energy calibrations of the instrument are performed using the well-known melting temperature and enthalpy of high purity indium. All the DSC scans were performed in a flowing N_2 atmosphere.

Thin films have been prepared on to well-cleaned glass substrates kept at room temperature by thermal evaporation method at a pressure less than 10^{-5} mbar [5]. The thickness of the films was measured by the Tolansky interference method and found to be 350 nm. The annealing of the pristine samples (powdered and thin films) have been performed in a running vacuum $\sim 10^{-5}$ mbar. A Philips X-ray diffractometer type-1710 was used to characterize the pristine and annealed samples. The surface morphology and composition analysis of the as prepared and annealed films was carried out on scanning electron microscope (Philips XL30 ESEM system with EDAX attachment) operated at 20 kV. The secondary electrons are collected for the surface morphology, while X-rays produced through the electron beam impact for the composition analysis are taken in the present study. The dc conductivity measurements were carried out in the temperature range 253–343 K in a running vacuum of $\sim 10^{-4}$ mbar. The current was measured using a digital picoammeter (DPM-111, Scientific equipment, Roorkee). The Al electrodes (electrode gap ~ 2 mm) in co-planar geometry were deposited by thermal evaporation for electrical measurements. The optical transmission spectrum was recorded at room temperature using a UV–VIS spectrophotometer in the wavelength range 500–1,100 nm.

Results and discussions

Thermal properties

Figure 1 shows the DSC scans of $Sn_{10}Sb_{20}Se_{70}$ glassy semiconductor at different heating rates. It is observed that the glass transition temperature (T_g) and peak crystallization temperature (T_p) increases with the heating rate. The lowering and broadening of the melting endotherm occurs with the heating rate. The glass transition temperature is 424.1 K and onset of crystallization temperature is 514.3 K at 10 K/min heating rate. Further, the X-ray diffraction patterns of powdered bulk samples as pristine, annealed below T_g and at peak crystallization temperature were compared and are shown in Fig. 2. These results show that the sample (a) and (b) are X-ray amorphous, while annealing at peak crystallization temperature shows the

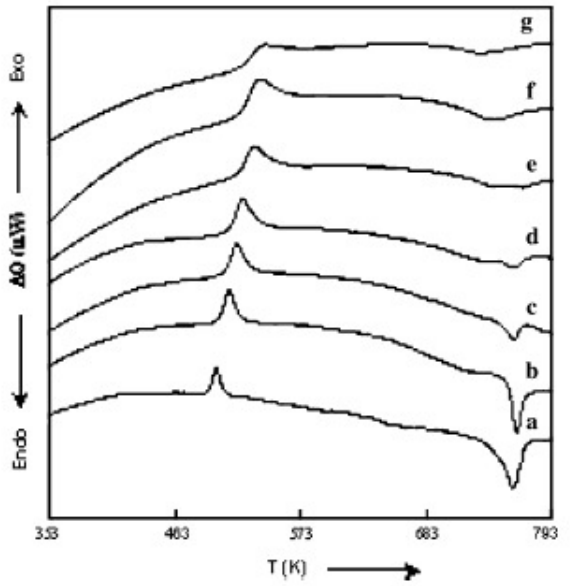

Fig. 1 DSC thermograms for amorphous $Sn_{10}Sb_{20}Se_{70}$ glasses at heating rates (a) 5, (b) 10, (c) 15, (d) 20, (e) 30, (f) 40, (g) 50 K/min

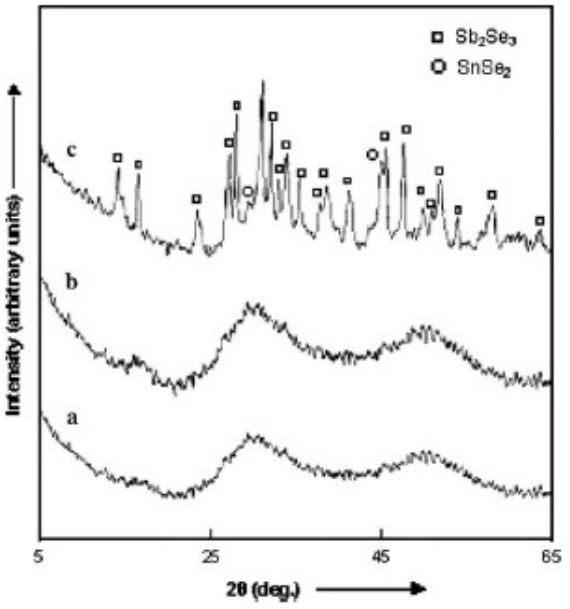

Fig. 2 X-ray diffraction patterns for pristine sample (a), annealed at 393 K (b) and annealed at 550 K for 1 h for $Sn_{10}Sb_{20}Se_{70}$ chalcogenide glass

crystalline nature for the sample (c). The formation of crystalline globule could be attributed to the large difference in the average bond energy of the constituent phase's, viz. Sb_2Se_3 and $SnSe_2$ as Sn forms the strong bonds. The percentage crystallinity for the as-prepared glass sample

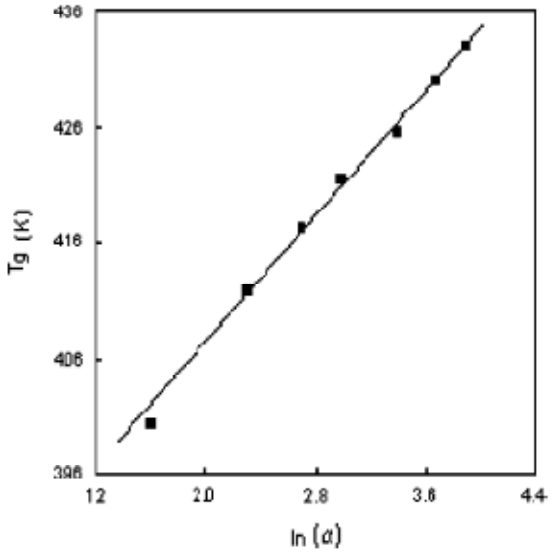

Fig. 3 Variation of T_g with heating rate for $Sn_{10}Sb_{20}Se_{70}$ glassy samples

was calculated from the heat evolved and heat absorbed during the crystallization and melting of the material, respectively. The heat evolved/absorbed at 10 K/min heating rate is 26.7 and 28.4 mJ/mg for the crystallization and melting peaks, which is found to be 0.38% for this glassy sample.

The difference $\Delta T = T_c - T_g$, representing the resistance to devitrification or thermal stability of glasses [6], has been found to be 90.2 K. The dependence of T_g on heating rate could be discussed by using the empirical relationship proposed by Lasocka as: $T_g = A + B \ln\alpha$, where A and B are constants for a given glass composition [7]. Figure 3 shows a plot of T_g vs. $\ln\alpha$ for $Sn_{10}Sb_{20}Se_{70}$ glassy semiconductor and the points could be best fitted to a straight line. Using the slope and intercept values, the above equation becomes: $T_g = (379 \pm 2) + (13.8 \pm 0.2)\ln\alpha$. The value of B depends on the cooling rate employed in the preparation and is the indicator of the response of the configurational changes within the glass transition region to the heating rate [8]. The apparent activation energy for glass transition E_t is calculated using the Kissinger equation [9]:

$$\ln(\alpha/T_g^2) = -E_t/RT_g + \text{constant} \quad (1)$$

where R is the gas constant. Figure 4a shows a linear variation of $\ln(\alpha/T_g^2)$ vs. $1/T_g$ for the investigated glass. From the slope of the straight line, the value of E_t is found to be 100.2 ± 0.4 kJ/mol. From the heating rate dependence of T_p, the activation energy for the crystallization process is calculated using the Kissinger equation as [9]:

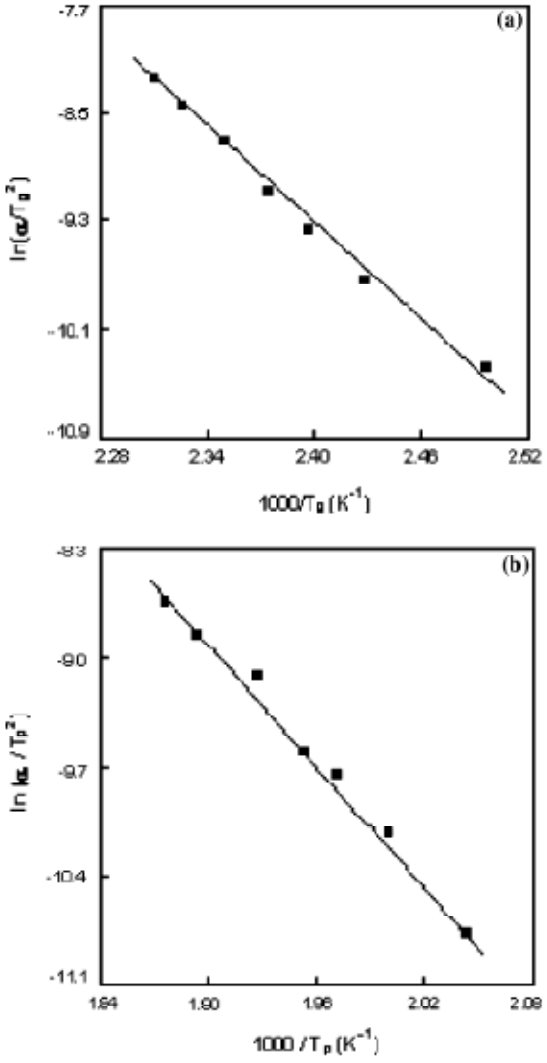

Fig. 4 The plots of (a) $\ln(\alpha/T_g^2)$ with $1{,}000/T_g$ and (b) $\ln(\alpha/T_p^2)$ with $1{,}000/T_p$ for amorphous $Sn_{10}Sb_{20}Se_{70}$ chalcogenide glass

$$\ln(\alpha/T_p^2) = -E_c/RT_p + \text{constant} \quad (2)$$

The value of E_c was obtained from the straight line plots of $\ln(\alpha/T_p^2)$ versus $1{,}000/T_p$ as shown in Fig. 4b. The value of E_c deduced as above is found to be 107.3 ± 0.4 kJ mol^{-1}.

Surface morphology

The surface morphologies of the pristine and annealed films (annealing temperature, $T_a = 400$ K) are shown in the Fig. 5a and b, respectively. The SEM micrograph shows a decrease in the surface roughness upon annealing,

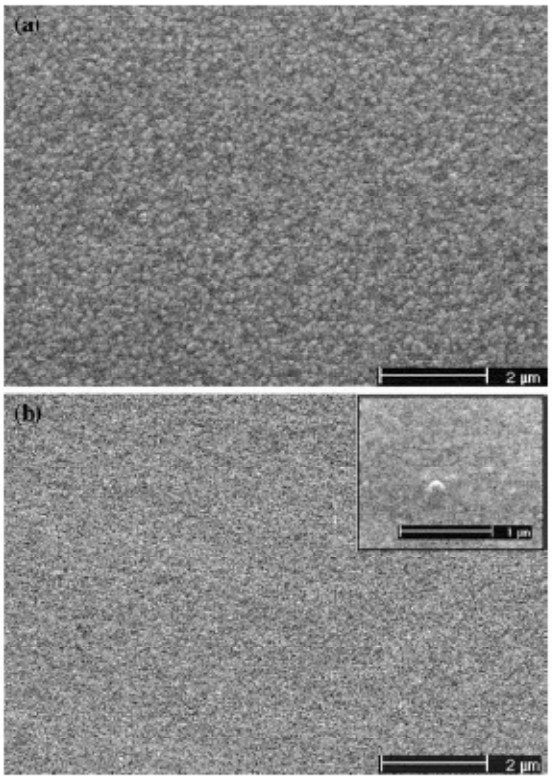

Fig. 5 The SEM micrographs for the pristine (a) and annealed at 393 K (b) for 1 h for amorphous $Sn_{10}Sb_{20}Se_{70}$ chalcogenide glass. The inset picture in Fig. 4b shows the enlarged image of the spherical globule in the amorphous matrix

while the 3D spherical globule appears in the amorphous matrix. The inset image in Fig. 5b shows the magnified image of one such globule for the annealed sample. The comparison of the SEM and XRD patterns suggests that these small globules might be the Sb_2Se_3 phase, as of its higher affinity toward the crystallization in the bulk glass samples.

Electrical conduction

The annealing of the pristine samples was carried out at 333, 363, and 393 K well below the glass transition temperature and the effect of the nucleation of crystallites on the electrical conduction has been investigated. The room temperature (303 K) conductivity is found to decrease with the increase in the annealing temperature (Table 1). The electrical conductivity of the thin films of $Sn_{10}Sb_{20}Se_{70}$ (pristine and annealed) as a function of temperature is shown in Fig. 6. It has been observed that the dark conductivity increases linearly with temperature in the range 253–343 K and follows the Arrhenius equation: $\sigma = \sigma_o \exp(-\Delta E/kT)$, where σ_o is the pre-exponential factor, ΔE is the dc activation energy, k is the Boltzmann constant, and T is the absolute temperature. From the slope and intercept on the y-axis of $\ln\sigma$ versus $1{,}000/T$ curves, the values of ΔE and σ_o were calculated for all the samples. The value of σ_o may distinguish whether the dominant conduction process is in the extended states or in the localized states. For extended state conduction, the value of σ_o lies in the range 10^3–10^4 S cm^{-1}, whereas for the hopping conduction in the localized states the value of σ_o is much smaller than this range [10]. As shown in Table 1, the value of σ_o for pristine sample is 8.9×10^3 S cm^{-1} and with annealing temperature the value of σ_o decreases to 0.2×10^3 S cm^{-1} for sample annealed at 393 K. Thus, annealing does not change the dominant conduction process, which remains in the extended states for $Sn_{10}Sb_{20}Se_{70}$ sample.

The small values as reported elsewhere [5] may be due to the electrode (Ag-electrode) or thickness effect, the exact details of which will be investigated in the future. The decrease in the value of σ_o is much higher for the annealing temperatures near the glass transition temperature. Generally, annealing reduces the concentration of the dangling and unsaturated bonds, which allow the structure to relax to a state closer to the equilibrium, thereby reducing the density of defect states. Mohamed et al. have attributed the increase in bulk roughness with annealing temperature to the grain growth and the stresses, which built up in the film during heating and subsequent cooling [11]. A decrease in the surface roughness occurs with the nucleation of crystalline Sb_2Se_3 globules in the amorphous matrix have been observed in the SEM micrographs. This increases the surface dangling bonds and unsaturated defects associated with these structures and thus leads to an increase in the density of defect states in the present system. Thus, there is an increase in the scattering centers and

Table 1 Dependence of some electrical and optical parameters on the annealing temperature for $Sn_{10}Sb_{20}Se_{70}$ film samples

Sample	E_o (eV)	B^{-1} ($\times 10^{-3}$ cm eV)	σ_{RT} ($\times 10^{-5}$ S cm^{-1})	ΔE (eV)	σ_o ($\times 10^{-3}$ S cm^{-1})
Pristine	1.13	1.84	8.89	0.49	8.9
$T_a = 333$ K	1.11	1.82	5.97	0.45	1.2
$T_a = 363$ K	1.06	1.79	5.27	0.42	0.5
$T_a = 393$ K	1.05	1.62	5.17	0.41	0.2

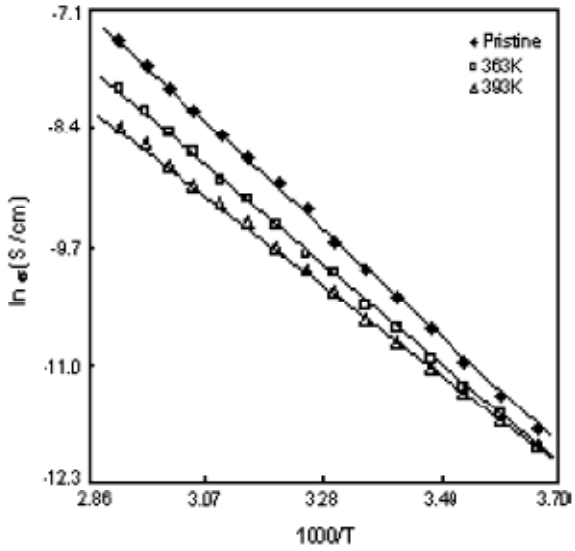

Fig. 6 Plot between lnσ versus 1,000/T for pristine and annealed $Sn_{10}Sb_{20}Se_{70}$ films

dangling bonds with annealing resulting in an increase in the density of defect states in the mobility gap.

The observed variation in σ_o can further be understood in terms of its variation with the ΔE, known as Meyer–Neldel rule. This rule is found to obey in various thermally activated phenomena, e.g., kinetics (hopping) and thermodynamics (number of carriers in the band state) in amorphous semiconductors, condensed matter physics, chemistry, biology, and geology [5, 12, 13]. This rule correlates σ_o and ΔE as: $\sigma_o = \sigma_{oo} \exp(\Delta E/E_{MN})$, where E_{MN} is the Meyer–Neldel characteristic energy and σ_{oo} is the prefactor, which is treated as the microscopic conductivity in these semiconductors. The plot of lnσ_o and ΔE (not shown here) can be best fitted to a straight line. The slope and intercept yields the values of $E_{MN} \sim 23.2$ meV and $\sigma_{oo} \sim 5.6 \times 10^{-6}$ S cm^{-1} for this glass. These values are found to be in good agreement with the published data [5, 12]. The validity of the MN-rule and obtained activation energies tells about the exponential distribution of tail states near the mobility edge as proposed by Roberts [14]. Thus, the major contribution of the conduction process does not come from the region of the Fermi level but more likely from these tail states. Hence, σ_o does not have a same value with annealing temperature, since position of these tail states are strongly influenced due to annealing. Therefore, the value of σ_o cannot be treated as microscopic conductivity but σ_{oo} can be. The small values of the prefactor can be attributed to the interlayer potential barriers, which restrict the motion of charge carriers in chalcogenide glasses [12].

Optical properties

The effect of thermal annealing on the optical properties was investigated by studying the transmission spectra for the pristine as well as for the annealed films. A decrease in the transmittance for the annealed films was observed. The decrease in the transmittance upon annealing was considered due to the nucleation of scattering centers or crystal growth (crystallization of Sb_2Se_3 as spherical globules) in the bulk of the material, however, the surface roughness decreases. The analysis of optical transmittance data has been used to discuss these features. In the high absorption region ($\alpha \geq 10^4$ cm^{-1}), involving indirect interband transitions between valence and conduction bands, α follows the relation: $\alpha = B(h\nu - E_o)^2/h\nu$, where E_o is the optical energy gap and B is an energy independent constant, which is a measure of the extent of band tailing [10]. Linear plots of $(\alpha h\nu)^{1/2}$ versus $h\nu$ are shown in Fig. 7. The optical gap (E_o) was calculated by taking the intercept on the energy axis and the value of B was calculated from the slope of the plots. The values are summarized in Table 1. An inverse relation between these two parameters has been observed.

According to Mott and Davis [10], the width of the localized states near the mobility edge depends on the degree of disorder and the defects present in the amorphous structure. The unsaturated bonds along with the saturated ones are present in the deposited film. These unsaturated bonds are responsible for the formation of defects, responsible for the localized states in the mobility gap of amorphous solids. Generally, annealing leads to a decrease in the density of these defect states due to thermal

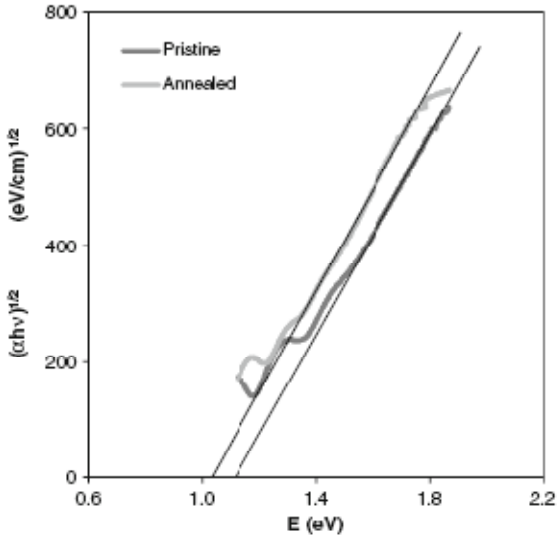

Fig. 7 The plots of $(\alpha h\nu)^{1/2}$ versus $h\nu$ for the pristine and annealed samples of $Sn_{10}Sb_{20}Se_{70}$ glass

relaxation and hence an increase in the optical gap of the material. In the present case, the decrease in the optical gap with annealing may be due to the nucleation of scattering centers. A decrease in the optical gap after annealing with the decrease in the thickness in the Ge based films has been reported [15]. Similar behavior has also been observed in Cu–Ge–Te and Ge–As–Te thin films and was attributed to the increase in the number of surface dangling bonds associated with the growing crystallites [16, 17]. These dangling bonds are probably responsible for the formation of some type of defects in the highly polycrystalline solids. As the number of dangling bonds and defects increase with annealing temperature, the concentration of localized states in the band structure increases gradually thereby reducing the optical gap.

It can be easily seen from the Table 1 that the difference between ΔE and E_o decreases with the annealing temperature with large difference for the sample annealed near the glass transition temperature. Since ΔE is not equal to half of the optical gap ($E_o/2$), the Fermi level is not located near the center of the gap. The observed change in the properties with annealing temperature can be interpreted in terms of the amorphous-crystallization transformation. During this transformation, thermally induced crystalline phase grows, which increases the density of surface dangling bonds associated with crystallites in the films matrix and causes a decrease in the electrical conductivity and consequently, a decrease in the activation energy for conduction. A shift in the Fermi level toward the valence band edge is observed with increase in annealing temperature. Annealing near the glass transition temperature results in the structural relaxation of the glassy network with consequent refinement of the gap states. The decrease in the conductivity observed thus can be due to the nucleation of the crystallites in the present system. Similar decrease in the properties has also been observed with annealing in Ge–Sb–Se system [18].

Conclusions

The calorimetric studies of the as prepared $Sn_{10}Sb_{20}Se_{70}$ glasses at different heating rate have been performed. The optical transmission, optical gap, and dc activation energy has been found to be annealing temperature sensitive. The nucleation of spherical globules of Sb_2Se_3 with the annealing near the glass transition temperature has been reported. The observed properties have been explained by considering the increase in the disorder with the nucleation of globular crystallites in the amorphous matrix.

Acknowledgements The authors wish to thank Mr. Jagtar Singh, Sophisticated Analytical Instrumentation Facility (SAIF), Punjab University, Chandigarh, and Mr. Jagdish Singh, Scientific Officer, Institute Instrumentation Center, IIT, Roorkee, for their timely help in the XRD and DSC studies, respectively.

References

1. Wang F, Boolchand P (2004) In: Lucovsky G, Popescu M (eds) Non-crystalline materials for optoelectronics, vol 1. INOE, Romania
2. Wang Z, Tu C, Li Y, Chen Q (1995) J Non-Cryst Solids 191:132. doi:10.1016/0022-3093(95)00249-9
3. Klocek P, Roth M, Rock RD (1987) Opt Eng 26:88
4. Kumar P, Thangaraj R (2006) J Non-Cryst Solids 352:2288. doi:10.1016/j.jnoncrysol.2006.02.041
5. Kumar P, Bindra KS, Suri N, Thangaraj R (2006) J Phys D Appl Phys 39:642. doi:10.1088/0022-3727/39/4/008
6. Mehta N, Agarwal P, Kumar A (2005) Eur Phys J Appl Phys 31:153. doi:10.1051/epjap:2005048
7. Lasocka M (1976) Mater Sci Eng 23:173. doi:10.1016/0025-5416(76)90189-0
8. Tichy L, Rysava N, Trisk A, Ticha H, Klikorka J (1984) Sol Stat Commun 49:903. doi:10.1016/0038-1098(84)90451-4
9. Kissinger HE (1956) J Res Natl Bur Stand 57:217
10. Mott NF, Davis EA (1979) Electronic processes in non-crystalline materials. Clarendon, Oxford
11. Mohamed SH, Kappertz O, Niemeier T, Drese R, Wakkad MM, Wuttig M (2004) Thin Solid Films 468:48. doi:10.1016/j.tsf.2004.04.017
12. Shimakawa K, Abdel-Waheb F (1997) Appl Phys Lett 70:652. doi:10.1063/1.118323
13. Yalon A, Movaghar B, Crandall RS (2006) Rep Prog Phys 69:1145. doi:10.1088/0034-4885/69/4/R04
14. Roberts GG (1971) J Phys C Solid State 4:3167. doi:10.1088/0022-3719/4/18/021
15. Kuzukawa Y, Ganjoo A, Shimakawa K (1998) J Non-Cryst Solids 227–230:715. doi:10.1016/S0022-3093(98)00192-6
16. El Zahed H (2001) Physica B (Amsterdam) 307:95. doi:10.1016/S0921-4526(01)00644-5
17. Mohamed SH, Wakkad MM, Ahmed AM, Diab AK (2006) Eur Phys J Appl Phys 34:165. doi:10.1051/epjap:2006061
18. Moharram AH (2004) Appl Phys A 66:515. doi:10.1007/s00339005070